nature communications

Article

https://doi.org/10.1038/s41467-024-54725-w

Engineering enzyme conformation within liquid-solid hybrid microreactors for enhanced continuous-flow biocatalysis

Received: 29 March 2024

Accepted: 20 November 2024

Published online: 30 November 2024

Check for updates

Xiaoting Hao[1,2,3,4], Shuo Wang[1,4], Xiaoming Zhang[1,3] ✉, Zhiqiang Ma[1], Ming Zhang[1,2], Hu Shi[1] ✉ & Hengquan Yang[1,2] ✉

The artificial engineering of an enzyme's structural conformation and dynamic properties to promote its catalytic activity and stability outside cellular environments is highly pursued in industrial biotechnology. Here, we describe an elegant strategy of combining the rationally designed liquid-solid hybrid microreactor with a tailor-made polyethylene glycol functional ionic liquid (PEG-IL) microenvironment to exercise a high level of control over the configuration of enzymes for practical continuous-flow biocatalysis. As exemplified by a lipase driven kinetic resolution reaction, the obtained system exhibits a 2.70 to 30.35-fold activity enhancement compared to their batch or traditional IL-based counterparts. Also, our results demonstrate that the thermal stability of encapsulated lipase can be significantly strengthened in the presence of PEG groups, showcasing a long-term continuous-flow stability even up to 1000 h at evaluated temperature of 60 °C. Through systematic experiment and molecular dynamics simulation studies, the conformational changes of the active site cavity in the modified lipases are correlated with enzymatic properties alteration, and the pronounced effects of PEG-groups in stabilizing enzyme's secondary structures by delaying unfolding at elevated temperatures are identified. We believe that this study will guide the design of high-performance enzymatic systems, promoting their utilization in real-world biocatalysis applications.

Biological cells have evolved a highly specific cellular environment, which affords on-demand programming of enzymatic conformations with extraordinary catalytic proficiency and specificity[1–4]. Inspired by this, the rational design and creation of artificial synthetic systems with altered spatial microenvironment has become one of the most promising ways to modulate the enzyme's structural conformation and dynamic properties in vitro[5–10]. As yet, various strategies ranging from chemical modification of the protein to the tailoring of host materials or reaction medium have been applied with varying success[11–17]. Among these methods, immobilizing enzymes on specific macromolecular scaffolds or spatial organizing enzymes within their engineered micro/nano-confined environments, like zeolites[18], mesoporous silica[19–21], metal-organic frameworks (MOFs)[22–25], covalent organic frameworks (COFs)[26–28] et al., has attracted especial attentions due to the intrinsic advantages in easy recovery and recycling of the enzyme, continuous production ability and simplified downstream processing. Those research efforts have showcased the capability of a favorable support or local microenvironment around enzymes in

[1]School of Chemistry and Chemical Engineering, Shanxi University, Taiyuan 030006, China. [2]Engineering Research Center of Ministry of Education for Fine Chemicals, Shanxi University, Taiyuan 030006, China. [3]Longzihu New Energy Laboratory, College of Chemistry and Molecular Sciences, Henan University, Kaifeng 475004, China. [4]These authors contributed equally: Xiaoting Hao, Shuo Wang. ✉e-mail: xmzhang4400@sxu.edu.cn; hshi@sxu.edu.cn; hqyang@sxu.edu.cn

promoting the catalytic efficiency, regulating the substrate selectivity or even improving the enzyme stability at harsh working conditions. Despite such intriguing advances, the full potential of microenvironment engineering strategy for industrial biotechnology still confronts difficult challenges[29–32]. On the one hand, most of the immobilized enzymes suffer from several common restrictions, including complex immobilization procedures, needing special matrix, and possible enzyme inactivation through uncontrolled conformational changes during the immobilization process. On the other hand, the traditional immobilized enzymes within host materials often lack conformational freedom or conformation flexibility because of the absence of desired liquid microenvironments in the existing synthetic systems. Moreover, fully exploiting the potential of immobilized enzymes in industrial biocatalysis requires not only the activation and long-term stabilization of catalytically active proteins under operational situations but also their integration into industrially preferred fixed-bed reactor systems. Thus, seeking a more elegant and practical synthetic cellular model to overcome these challenges of current approaches is still in urgent demand.

Alternatively, ionic liquids (ILs) as a powerful tool to improve enzymatic organic synthesis has been proposed for a long time ago considering their intriguing properties like less-volatile, low toxicity and unique solubility[33,34]. So far, tremendous efforts have already been directed to address the effect of ILs diversity (like cation and anion types, functional groups, biocompatible deep eutectic solvent) on the structure and function of enzymes in biphasic systems, triggering enhanced enzyme activity or thermal stability by flexible choosing suitable ILs[35–39]. Meanwhile, to solve the problems encountered in traditional biphasic IL system (high viscosity, large diffusion distance, batch reaction manner), several immobilization methods including supported-IL phase (SILP) system, entrapped IL system and IL gel system have also been intensively explored[40–44]. More recently, our group conceptually developed a liquid–solid hybrid microreactor-based catalytic system, in which the homogeneous biocatalyst together with its IL microenvironment were simultaneously entrapped within a solidified porous crust[45]. Such a designed catalyst features a unique structure that comprising a micron-scaled liquid pool and a permeable silica shell, enabling the integrated specialities of both enzyme immobilization (e.g. mechanical strength, continuous-flow operation) and homogeneous biocatalysis (e.g. good activity, conformational freedom). Moreover, regulable catalysis efficiency and long-term continuous flow stability were fulfilled by rational engineering the parameters of solid crust or liquid pool while directly packing the hybrid catalyst into a fixed-bed column reactor. Expectedly, given the fully customizable nature of interior ILs, there is a broader scope for further upgrading the catalytic performance of this hybrid microreactor to a practically applied level. However, different from the physiological liquid environments, biocatalysts are often unstable in traditional hydrophilic ILs or poorly soluble in hydrophobic ILs, causing a severe trade-off between enzymatic activity and stability. Although amphiphilic ILs have been exploited to resolve this problem, the biphasic batch reaction is often hindered by the product inhibition effect, leading to a low level of catalytic effectiveness[46–48]. Besides, the interplay between adopted ILs microenvironment and enzyme's structural conformations is still not fully understood up to now. In this context, an in-depth and comprehensive study on the local microenvironment engineering of the liquid-solid hybrid microreactor is highly desired, so as to meet the harsh requirement of industrial production processes.

With this objective in mind, we here utilize a task-specific polyethylene glycol functional ionic liquid (PEG-IL) as a positive modulator to draw accurate control over the configuration of the confined enzyme within the liquid-solid hybrid microreactors. The attractiveness of using this type of IL instead of other ones, stems from the inherent specialities of PEG groups, including excellent ability to solvate range of organic substrates, good enzyme solubility, high hydration and flexibility, which may work synergistically with thus ILs to construct a desired local microenvironment for the encapsulated enzymes. In doing so, we have been able to significantly push the optimal catalytic capability of these promising IL-based microreactors. As exemplified by a lipase driven kinetic resolution reaction, reinforced activity and thermostability are validated in an industrially preferred continuous-flow catalysis manner. More interestingly, the catalytic efficiency can be modulated by precisely tuning the molecular weight of PEG groups, thus enabling a molecular-level control of the enzymatic activity, which is hard to be accomplished by traditional immobilization methods. Through a combination of experimental methods and molecular dynamics (MD) simulations, a comprehensive understanding of the effect of PEG-IL molecules on the catalytic activity and conformational changes of enzymes are elucidated, and the pronounced effects of PEG-groups in stabilizing enzyme's secondary structures by delaying unfolding at elevated temperatures are identified. This work showcases the conception of modulating an enzyme's conformation in a confined media, which offers new insights to guide the design of highly efficient biocatalysts for practical applications.

Results

Construction of the task-specific PEG-IL-based liquid-solid hybrid microreactor

Similar with our previous report[45], the whole synthetic method involves a primary emulsification step and an interfacial cross-linking process around the formed Pickering droplets (as illustrated in Fig. 1). A series of functionalized ILs, $[PEG_m(mim)_2][NTf_2]_2$ (m represents molecular weight of PEG groups, m = 200, 600 or 1000), composed of a hydrophilic PEG bridged methylimidazolium cation and a hydrophobic bis(trifluoromethanesulfonyl) imide anion ($[NTf_2]$), were synthesized (for ^{1}H-NMR and ^{13}C-NMR, Supplementary Fig. 1) and used as the dispersed phase. Hydrophobic silica nanoparticles, which were got by simply modifying a commercial silica (20 nm in size, Wacker Chemie) with a certain amount of dimethyldichlorosilane, were screened as the solid emulsifier (for details and characterizations, Supplementary Fig. 2). *Candida antarctica* lipase B (CALB), a most widely used enzyme in academic and industrial laboratories, was chosen as a model for this study. After vigorously homogenizing a mixture of PEG-IL that dissolved with CALB and oil phase (*n*-octane) that dispersed with silica emulsifier, an IL-in-oil Pickering emulsion was formulated. Taking $[PEG_{600}(mim)_2][NTf_2]_2$ as an example, the formed droplets are discrete and spherical in morphology with a relatively uniform size distribution of 31 μm (Fig. 2a). Preferential assembly of silica emulsifier at the droplet interface was verified by a fluorescence dyeing experiment using fluorescein isothiocyanate isomer I (FITC-I) labelled silica as an emulsifier, which presented a fluorescent circle around the droplet surface in the 2D or 3D confocal fluorescence microscopy (CLSM) images (Supplementary Fig. 3). After dyeing CALB enzyme with Rhodamine B, red fluorescence signals are clearly seen throughout the whole droplet interior (Fig. 2b, c and Supplementary Fig. 4), suggesting that enzymes are perfectly encapsulated and homogeneously distributed within the IL-in-oil type emulsion droplets. Notably, almost no variation of the fluorescence intensity was observed for these droplets over a time period of one day (Fig. 2d and Supplementary Fig. 5), suggesting the excellent confining ability of the task-specific PEG-IL droplets toward enzymes. For the following interfacial growth process, a hydrophobic silica precursor, methyltrimethoxy silane (MTMS), that are initially existed in the continuous oil phase and can be hydrolyzed under mild conditions, was utilized. After an interfacial sol–gel process, a silica crust around the Pickering droplets was built up, yielding the aimed PEG-IL-based liquid-solid hybrid microreactor.

Scanning electron microscopy (SEM) images reveal that the obtained hybrid material comprises intact spherical microcapsules

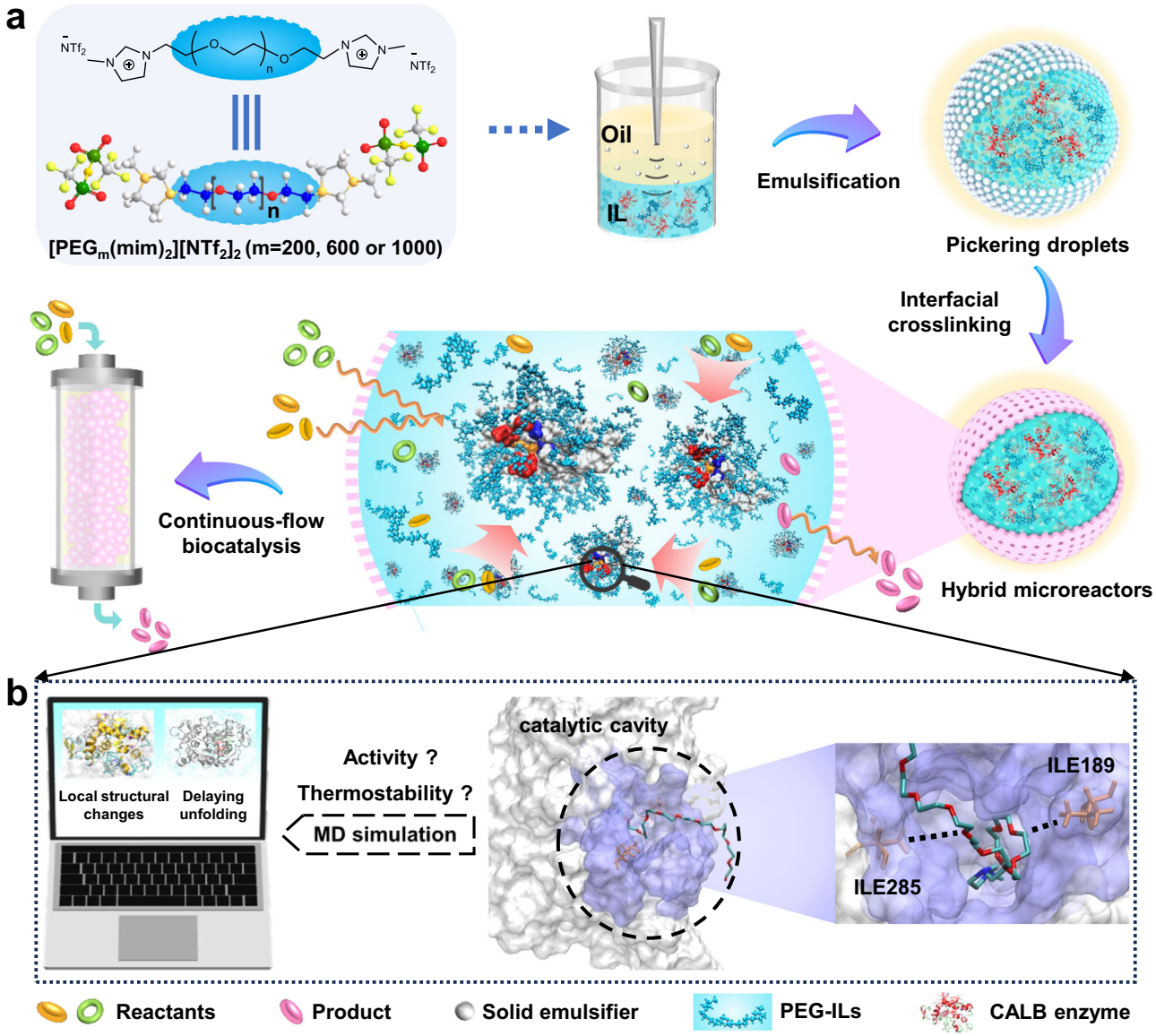

Fig. 1 | A schematic diagram illustrating the construction of liquid–solid hybrid microreactors with a task-specific PEG-IL microenvironment for enhanced continuous-flow biocatalysis. a General synthesis process of the designed microreactor, **b** theoretical calculation illustration.

with a similar particle size with the droplets, of which the external surfaces are relatively smooth and decorated with silica emulsifiers (Fig. 2e, f). After removing interior PEG-IL with polar solvent, its hollow structure is clearly visible from the observation of an individual cracked particle, confirming the interfacial growth of MTMS (Fig. 2g). Further magnified the cross-sectional view of the outer boundary, it was found that the formed silica crust is dense and continuous with a thin thickness of 70 nm (Fig. 2h), due to an interfacial self-completing growth mechanism[49]. Transmission electron microscopy (TEM) observation shows the existence of irregular mesopores in the outer crust, which enables the accessible mass transport during catalytic processes (Fig. 2i). Elemental mappings appear uniform distributions of C, Si, O, N, F and S throughout the whole microreactor (Fig. 2j), indicating the successful encapsulation of both PEG-IL and CALB enzymes. To clarify the thermal stability and loading content of PEG-IL in the hybrid material, thermos-gravimetric analysis (TGA) was then conducted. As exhibited in Fig. 2k, only a slight weight loss that ascribing to the physically adsorbed water was observed before 200 °C. A major weight loss between 200 and 600 °C reached up to 87.0%, which can be attributed to the decomposition of PEG-IL. Such a high-loading content is meaningful for the realization of real homogeneous process within the hybrid microreactors. The porosity of the microcapsules was also characterized by a N_2 sorption analysis. As shown in Fig. 2l, the empty capsules display a type IV isotherm together with a H4-type hysteresis loop, which are characteristics of a mesoporous structure. The BET surface area and pore volume were determined to be 68.9 $m^2\ g^{-1}$ and 0.175 $cm^3 g^{-1}$ respectively. The pore size distribution calculated from a BJH method further confirmed the existence of mesopores at 4.41 nm. These mesopores might be originated from the interfacial sol-gel growth of silica in the presence of PEG-ILs.

As expected, such a synthetic method is applicable to a diversity of ILs. As shown in Supplementary Fig. 6, by tuning the molecular weight of PEG groups in $[PEG_m(mim)_2][NTf_2]_2$ or using traditional $[EMIM]NTf_2$, a range of Pickering droplets that are similar in morphology and size were produced. Attributing to the template effects, their corresponding hybrid microreactors also showed no significant difference in particle size (ranging from 29 to 31 μm) and crust thickness (ranging from 68 to 73 nm), as verified by the SEM images of the formed capsules at low magnification and the magnified views of their

https://doi.org/10.1038/s41467-024-54725-w

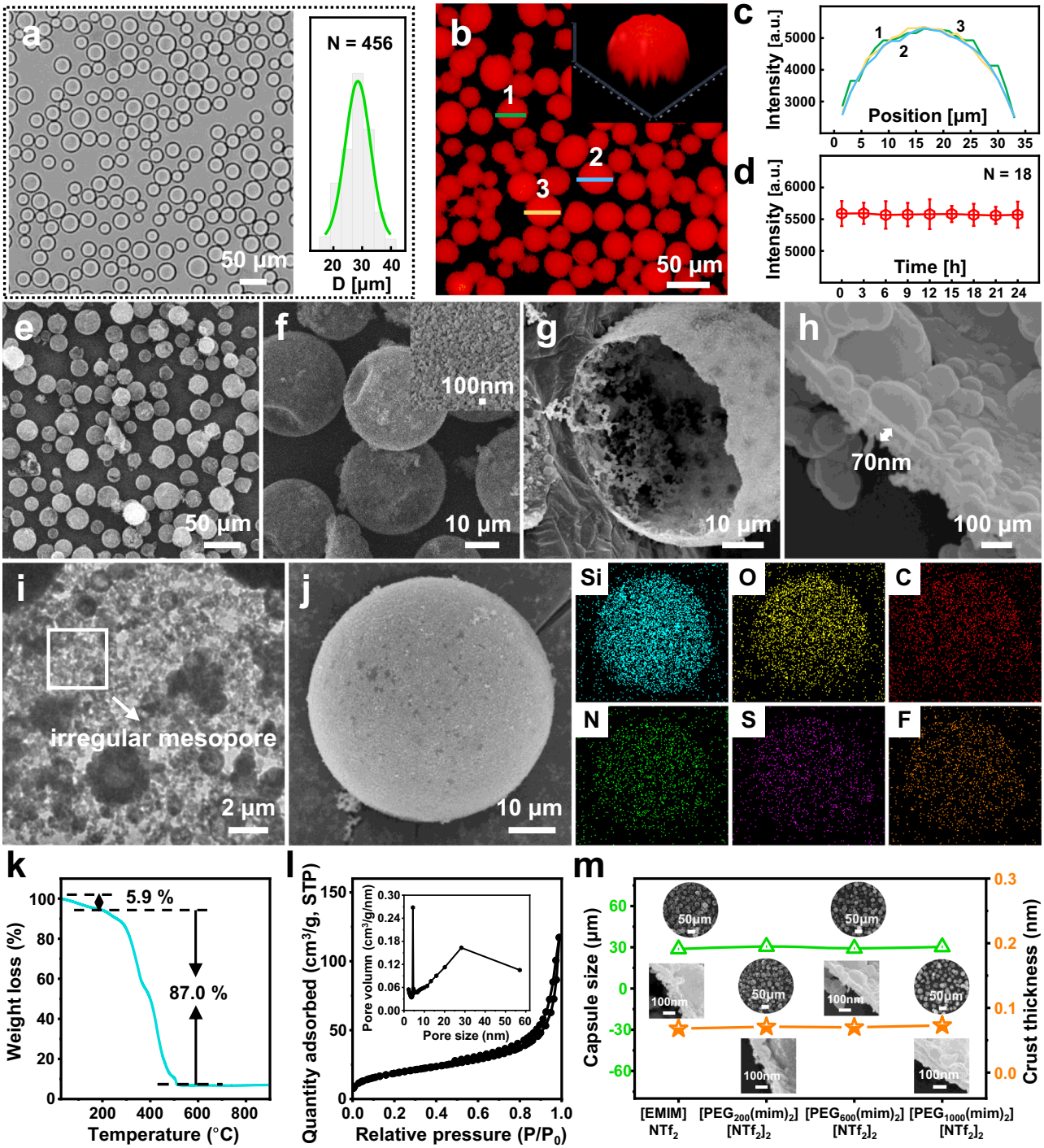

Fig. 2 | Characterizations of the PEG-IL-based liquid–solid hybrid microreactor. **a** Optical microscopy image of the formed Pickering droplets and their corresponding size distribution ($[PEG_{600}(mim)_2][NTf_2]_2$ as the IL phase). **b** Confocal fluorescence microscopy image of the emulsion droplets loading with Rhodamine B-dyed CALB, inset shows a 3D image. **c** Fluorescence intensity measured along the centerline of three droplets. **d** Fluorescence intensity variation over time (error bars represent standard deviation, N is the statistic droplet number). **e**–**h** SEM images of the microreactor: **e** a low magnified image, **f** several discrete capsules, inset shows the outer silica emulsifier, **g** a single broken particle, **h** a cross-sectional view of outer crust. **i** TEM image of a segment of the outer crust. **j** Element mappings of C, Si, O, N, S and F. **k** TGA curve. **l** N_2 sorption isotherms and BJH pore size distribution. **m** Average capsule size and outer shell thickness for different PEG-IL-based hybrid microreactors.

outer boundary (Fig. 2m and Supplementary Fig. 7). These hybrid materials possess a comparable loading content of interior IL, as confirmed by the close weight losses between 200 and 600 °C in their TGA curves (Supplementary Fig. 8). Interestingly, the weight loss before 200 °C is obviously decreased along with the decrease of PEG groups in $[PEG_m(mim)_2][NTf_2]_2$, which might be induced by the varied hydrophobicity/ hydrophilicity against PEG proportion that determined the physically adsorbed water. N_2 sorption analysis further demonstrated the porosity of these microcapsules, of which a type IV isotherm and pore size distributions centred at 4.41 nm were observed (Supplementary Fig. 9). The BET surface areas and total pore volumes are comparative ranging from 90.4 to 77.3 and 48.5 $m^2 g^{-1}$ and 0.193 to

0.146 and 0.153 $cm^3 g^{-1}$, respectively (Supplementary Table 1). From these above results, we can see that liquid-solid hybrid microreactors with a similar structure but different IL interior could be achieved, thus enabling a possible univariate study of the local microenvironment on the catalytic performance.

Encapsulation ability, mechanical stability and molecular permeability

Distinct from pure hydrophobic IL, the introduction of PEG groups is an effective way for the solubilization of enzymes, since the possible formation of PEG-lipase complex that arising from the existed interactions between proteins and PEG groups[50,51]. As shown in Supplementary Fig. 10, fluorescence-labeled CALB enzymes were observed homogeneously throughout the whole task-specific $[PEG_m(mim)_2][NTf_2]_2$ based microreactors, even at a high enzyme loading quantity, indicating the good encapsulation ability of PEG-IL toward enzymes. In contrast, phase separation phenomenon was observed for the PEG-free $[EMIM]NTf_2$-based microreactor under similar conditions, as verified by the appearance of some dark regions inside the microreactor. Apart from this, we also investigated the mechanical stability and molecular permeability of the hybrid microreactor, both of which are critical factors for the following biocatalysis applications. The mechanical stability was examined by packing the fabricated microreactors into a fixed-bed reactor, and pumped an oil phase through it at a relatively high velocity (15 mL h^{-1}) under 0.60 MPa pressure. As shown in Supplementary Fig. 11, the flow velocity kept constant over a period of 100 h, and almost no IL was leaked from the outlet as verified by the maintained height of packed column and unchanged weight losses (92.45%) after the flowing test. After this treatment, the discrete and spherical structures of the microcapsules were well preserved, further confirming their mechanical stability under flowing liquid conditions. Notably, a constant flow velocity was applicative for all the hybrid microreactors with diverse IL interior, even at a relatively high temperature of 80 °C (Supplementary Fig. 12, 13). Such a good stability might originate from the protection of silica skeleton around the droplets, which provide a sturdy shield for the internal PEG-IL. Meanwhile, the molecular permeability of the hybrid microreactors was evaluated by a fluorescence monitoring experiment. Nile Red (NR), as a fluorescent probe, was employed to visualize the molecular diffusion process. As shown in Supplementary Fig. 14, upon immersing the hybrid microreactors in this dye solution, a time-dependent CLSM variations were immediately recorded. The dye molecules that initially exist in the external surrounding, are observed to gradually pass through the silica crust and sequestered into the PEG-IL interior as time prolongs. Within only 10 s, fluorescent signals were clearly seen inside the microreactors, and the fluorescent intensity increases significantly in the subsequent 0.5-2.0 min, indicating the fast and smooth molecular diffusion ability. Interestingly, the fluorescent results of the hybrid microreactors with different IL interior showed that the rate of molecular diffusion was correlated with the molecular weight of PEG groups. As the molecular weight increased, the rate decreased in some degree, as proved by the slower increasing of fluorescent intensity inside the microreactor. This finding might be related with the increased viscosity of the task-specific IL with larger PEG molecular weight (Supplementary Fig. 15), which seriously impacts the molecular diffusion ability.

Catalytic activity enhancement

Next, we explored the potential of our task-specific PEG-IL-based hybrid microreactors in upgrading the enzymatic catalysis with a continuous-flow manner. The kinetic resolution of racemic alcohols, which is an important way to industrially produce chiral esters and alcohols[52], was examined. To conduct the reaction, the hybrid microreactors were packed into a fixed-bed reactor (for the setup, see Supplementary Fig. 16), and a solution of racemic alcohols and acylation reagent in *n*-octane was pumped into the reactor at a steady flow velocity. For comparison, the catalytic activity of conventional biphasic system and hybrid microreactor-based batch system were also evaluated (Fig. 3a_1). As exhibited in Fig. 3a_2, using racemic 1-phenylethyl alcohol as substrate, the ee values of alcohol gradually increased up to 90.5% while the corresponding ee values of ester product were always kept at 99% in the continuous-flow system. According to the steady values, the specific activity (SA) of CALB in this system was estimated to be 4.36 U mg^{-1}. In contrast, only 4.8% ee value of alcohol was achieved after 2 h in the conventional biphasic system, which would not increase further by prolonging the reaction time (Fig. 3a_3). On the basis of this value, the SA of biphasic system was calculated to be 0.378 U mg^{-1}. As for the hybrid microreactor system in batch, the ee value of alcohol reached 6.2% after the same period (Fig. 3a_4) and the SA was estimated to be 0.611 U mg^{-1}, which are slightly higher than that for the conventional biphasic system. Obviously, these catalytic results underline enhancement in catalytic efficiency of our hybrid microreactor based continuous-flow system, showing up to 11.5 and 7.1-fold acceleration on the catalytic rate than the biphasic system and hybrid microreactor based batch system (Fig. 3a_5). We believe this enhancement is mainly attributed to the continuous-flow effect that leads to timely removal of the product from the reaction system, which has been proved in our previous study[42]. In addition, the segmented IL droplets with enlarged interfacial area in this hybrid system might also contribute to the enhanced activity[53–56], since the intensified mass-transfer or molecular diffusion as confirmed by fluorescent dye uptake experiments. Notably, such catalytic activity of our hybrid microreactor is comparable or even much better than other enzyme immobilization systems, like commercial Novozym 435, mesoporous silica immobilized enzyme (SBA-15 as a support) and traditional supported IL systems (Supplementary Fig. 17), further highlighting the superior performance of our enzymatic hybrid microreactor system.

Having verified the superiority of our continuous-flow catalytic system, we then focused to study the effect of interior IL microenvironment on the catalytic activity. As shown in Fig. 3 (b_1 and b_2), under identical conditions, the final steady ee values of alcohol product differ considerably, depending on the molecular weight of PEG groups in $[PEG_m(mim)_2][NTf_2]_2$. As the molecular weight increased from 200 to 600 and 1000, the steady ee value of the alcohol increased from 85.9 to 91.5% and then decreased down to 46.2%, while the corresponding SA of the enzyme increased from 3.37 to 4.36 U mg^{-1} and then decreased to 2.92 U mg^{-1}. Interestingly, all of these task-specific hybrid catalysts exhibited markedly higher activity than the traditional $[EMIM]NTf_2$ (14.2% of steady ee value and 1.08 U mg^{-1} of specific activity), demonstrating the positive effects of PEG groups in upgrading the catalytic efficiency. To get a more comprehensive comparison, the catalytic performance of CALB in these hybrid microreactors with varied substrate concentration (from 0.05 to 0.4 M, the concentrations are different with each other since the distinct catalytic activity) was also evaluated. As shown in Fig. 3c and Supplementary Fig. 18, along with the increasing of substrate concentration, the steady ee values of the alcohol decreased from 90.5 to 69.8% for $[PEG_{600}(mim)_2][NTf_2]_2$ (0.10, 0.20 and 0.40 M), from 76.8 to 61.6% for $[PEG_{200}(mim)_2][NTf_2]_2$ (0.05, 0.10 and 0.20 M), from 59 to 39.8% for $[PEG_{1000}(mim)_2][NTf_2]_2$ (0.05, 0.10 and 0.20 M) and from 29.4 to 14.2% for $[EMIM]NTf_2$ (0.05, 0.075 and 0.10 M), while the corresponding SA values increased from 4.36 to 15.19, 2.01 to 7.03, 1.72 to 5.22 and 0.863 to 1.08 U mg^{-1} respectively. This pronounced concentration-dependent effect is not so difficult to be understood. At a low concentration, the substrate molecules are far less than the processed capacity of enzymes, thus leading to a high steady ee value but low specific activity. However, as the concentration increases, an increasing number of substrate molecules will not participate in the catalytic process. According to the above results, we further calculated

https://doi.org/10.1038/s41467-024-54725-w

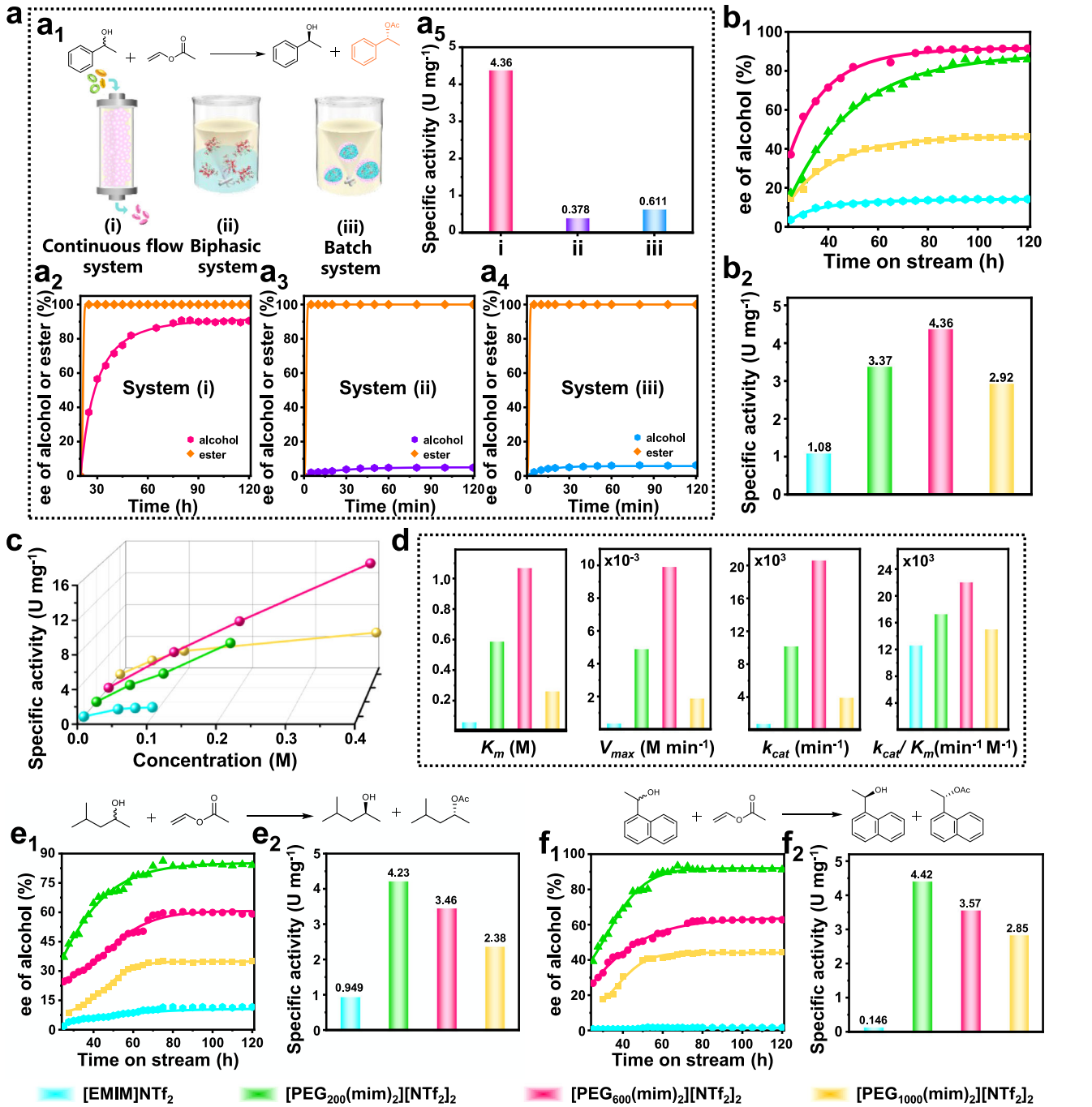

Fig. 3 | Catalytic performance of the liquid–solid hybrid microreactors. **a** Comparison of different catalytic systems in the kinetic resolution reaction of 1-phenylethyl alcohol, $\mathbf{a_1}$ schematic illustration of the different catalytic systems, $\mathbf{a_2}$–$\mathbf{a_4}$ Kinetic profiles for different catalytic systems: $\mathbf{a_2}$ hybrid microreactor based continuous-flow system; $\mathbf{a_3}$ conventional biphasic system; $\mathbf{a_4}$ hybrid microreactor system in batch, $\mathbf{a_5}$ comparison of the catalytic efficiency for different catalytic systems. **b** Impact of the different IL interior on the catalytic efficiency, including $[PEG_m(mim)_2][NTf_2]_2$ (m = 200, 600 or 1000) and $[EMIM]NTf_2$, (b_1, alcohol ee values with time; b_2, their specific activity). **c** Specific activity of the hybrid microreactors with different IL interior at varied substrate concentrations. **d** Comparison of K_m, V_{max}, k_{cat} and k_{cat}/K_m for CALB in the hybrid microreactor with different IL interior. **e**, **f** Comparison of the kinetic resolution of 4-methyl-2-pentanol or 1-(1-naphthyl)ethanol over the liquid–solid hybrid catalysts with different IL interior. ($\mathbf{e_1}$, $\mathbf{f_1}$: alcohol ee values with time; $\mathbf{e_2}$, $\mathbf{f_2}$: their specific activity). U is expressed as μmol of substrate converted per min (i.e. μmol min^{-1}). Batch reaction conditions are included in the Experimental Section of Supporting Information. Continuous flow biocatalysis conditions: 3.0 g liquid–solid hybrid microreactor, alcohol substrate (0.1 M), vinyl acetate (0.4 M) in *n*-octane, 45 °C, flow velocity 2 mL h^{-1}.

the kinetic parameters of CALB in these hybrid microreactor based continuous-flow systems (Supplementary Fig. 19), including the apparent Michaelis–Menten constant K_m (affinity of the enzyme to the substrate), the maximal reaction rate V_{max} and the turnover number k_{cat}. It was found that $[PEG_{600}(mim)_2][NTf_2]_2$ exhibited a higher catalytic power (higher V_{max} and k_{cat}) but a lower affinity for the substrate (higher K_m) (Fig. 3d). Specifically, the V_{max} in the $[PEG_{600}(mim)_2][NTf_2]_2$ based catalytic system was 9.9×10^{-3} M min^{-1}, which is 2.0, 5.2 and 26.8-fold higher than the other hybrid microreactors (4.9×10^{-3}, 1.9×10^{-3} and 0.37×10^{-3} respectively), while the k_{cat} for $[PEG_{600}(mim)_2]$

$[NTf_2]_2$ based catalyst was determined to be 2.0-26.8 fold higher than other hybrid microreactors. Notably, the K_m value of $[PEG_{600}(mim)_2][NTf_2]_2$-based catalytic system was estimated to be 1.068 M, which is also 1.8, 4.1 and even 17.5-fold higher than $[PEG_{200}(mim)_2][NTf_2]_2$, $[PEG_{1000}(mim)_2][NTf_2]_2$ and $[EMIM]NTf_2$, indicating a weaker binding affinity of CALB toward the alcohol substrate. To clarify the enhanced activity, the catalytic efficiency k_{cat}/K_m, a parameter of how efficiently an enzyme can convert substrate into product, was then calculated. As exhibited, the k_{cat}/K_m of $[PEG_{600}(mim)_2][NTf_2]_2$ based catalytic system was determined to be 22.0 min^{-1} M^{-1}, significantly higher than other systems i.e. $[PEG_{200}(mim)_2][NTf_2]_2$ (17.3 min^{-1} M^{-1}), $[PEG_{1000}(mim)_2][NTf_2]_2$ (15.1 min^{-1} M^{-1}) and $[EMIM]NTf_2$ (12.6 min^{-1} M^{-1}). Therefore, although the enzyme possesses a lower affinity for the substrate in $[PEG_{600}(mim)_2][NTf_2]_2$, the overall activity could still be improved by a higher turnover number (k_{cat}) and higher catalytic efficiency (k_{cat}/K_m). Moreover, the observed better performance when K_m is higher may also point towards the retention of the substrate and product due to the variant material properties, which could have a greater effect on an enzyme with a high affinity for organic chemicals. These significant differences in the kinetic parameter further confirm that the catalytic efficiency could be tuned by engineering the local IL microenvironment, and the anchored PEG groups provide opportunities to optimize the targeted catalytic activity.

Moreover, the positive effect of PEG groups was further validated by the kinetic resolution of other racemic alcohols including 4-methyl-2-pentanol and 1-(1-naphthyl)ethanol. As shown in Figs. 3e and 3f, a similar trend of catalytic activity was gained for these substrates except that the hybrid microreactor with a $[PEG_{200}(mim)_2][NTf_2]_2$ interior afforded the optimal performance. For example, using 4-methyl-2-pentanol as a substrate, about 84.0% of steady ee values and 4.23 U mg^{-1} of SA were achieved for the $[PEG_{200}(mim)_2][NTf_2]_2$-based hybrid catalyst, while 59.1, 35.0, 11.6% of steady ee values and 3.46, 2.38, 0.949 U mg^{-1} of SA were obtained for $[PEG_{600}(mim)_2][NTf_2]_2$, $[PEG_{1000}(mim)_2][NTf_2]_2$ and $[EMIM]NTf_2$. Interestingly, upon further inspection of a larger 1-(1-naphthyl)ethanol, we found that the task-specific hybrid catalysts expressed significantly promoted activity than the PEG-free one: 44.6-91.6% of steady ee and 2.85-4.42 U mg^{-1} of SA values for PEG-IL-based catalysts versus 1.60% and 0.146 U mg^{-1} for $[EMIM]NTf_2$ based catalyst. These results definitely indicate the crucial role of PEG-groups in affecting the enzyme performance and that the impacts on different substrates are not always the same.

To identify the underlying mechanism of the above catalytic activity, we then conducted all-atom MD simulations and spectroscopic analysis to address the effect of PEG groups on the structural or dynamical changes of CALB enzyme. For clearer exhibition and more robust understanding, the identical groups of methylimidazolium cation and $[NTf_2]$ anion were overlooked, while cluster structures (the cluster analysis details can be found in the Supplementary Information section) of three independent MD simulations per system were performed. The analysis mainly focused on the geometrical properties particularly the active site region of CALB and the interactions of substrate molecules with enzyme. As shown in Fig. 4a, the overall backbone structure of CALB is maintained in different IL microenvironment throughout the whole simulations. To provide insight into the structural changes, the root-mean-square deviation (RMSD) of the backbone atoms of CALB were calculated with respect to the initial frame of the simulations (Fig. 4b), in which all of the deviation ranges are less than 3.0 Å irrespective of the IL diversity, indicating the stability of CALB in these IL microenvironments. The RMSD value in $[EMIM]NTf_2$ shows a little higher than task-specific PEG-ILs, suggesting the stabilizing effects of PEG groups. Moreover, to assess the flexibility of CALB in these different ILs, the averaged RMSD for each residue was calculated. As exhibited in Fig. 4c, the averaged RMSD values of individual residues show distinct conformational flexibility in several regions including the α5 helix (residue 138 − 152), α10 helix (residue 268 − 287), L11 loop (residue 184 − 207) and L13 loop (243 − 267). The observed relatively high averaged RMSD for the α5 and α10 helices are interesting, since these regions are located at the entrance of the active site cavity that play a pivotal role in enzyme function as previously described[57–59]. To follow the conformation changes, fluorescence spectroscopy was then performed, which is reflected by the maximal intensity of the fluorescence (I_{max}) and the shift in the maximal emission wavelength (λ_{max}). As shown in Fig. 4d, the CALB in PEG-ILs exhibited red-shifts in λ_{max} (from 319 to 334 nm) and significant increase in I_{max} compared with $[EMIM]NTf_2$, suggesting a more rigid structure after exposing enzymes to an altered microenvironment. Interestingly, the florescence intensities of CALB gradually increased upon the increasing of PEG components, which confirms a more compact and flexibility reduced conformation with high levels of activity in the presence of specific PEG groups[48,60]. Further insight into the conformation changes of the CALB enzyme was also achieved using CD spectroscopy. As shown in Fig. 4e, the spectra of CALB differ according to the assayed medium, and characteristic minimum bands were appeared at 207 and 224 nm in all cases. However, there was a reduction in the CD spectra minima in $[EMIM]NTf_2$ with respect to the task-specific PEG-ILs, indicating that the enzyme possesses a particularly different secondary structure in each condition. As summarized in Supplementary Table 2, the α-helix content in the presence of PEG groups was higher compared with the pure hydrophobic $[EMIM]NTf_2$, which might impact the active site of the enzyme by stimulating higher tendency for the open conformation. Given that ILE285 and ILE189 are responsible for the open and closed conformations of the catalytic cavity and can regulate the substrate passage into the catalytic site in CALB, the structural changes of this helical region were further studied by MD simulations. As shown in Fig. 4f, g, the positions of these two residues (the mass center of the residues ILE189 and ILE285) in various ILs can change significantly and the distance between them is ranked in the following order: $[EMIM]NTf_2$ (16.5 Å) > $[PEG_{200}(mim)_2][NTf_2]_2$ (14.2 Å) > $[PEG_{600}(mim)_2][NTf_2]_2$ (13.4 Å) > $[PEG_{1000}(mim)_2][NTf_2]_2$ (11.7 Å). In comparison with the initial crystal structure (11.4 Å), the entrance distance of CALB in $[EMIM]NTf_2$ varied more greatly, since the absence of protection effects of PEG groups toward the enzyme conformation. Further secondary structure analysis (Supplementary Fig. 20) also displays larger deviation of the enzyme structure in $[EMIM]NTf_2$ compared with task-specific $[PEG_m(mim)_2][NTf_2]_2$, confirming the distinct conformational changes in these ILs as already verified by the fluorescence spectra and CD spectra analysis. Such drastic conformational changes may not favor the function expression of CALB, thus leading to deteriorated catalytic activity for $[EMIM]NTf_2$-based hybrid microreactor. Notably, it seems that the introduction of proper PEG groups is beneficial for the active gate conformations, featuring with relatively larger entrance size compared to the initial crystal structure. However, too long PEG groups will cause obstacles around the domain near the active site (Supplementary Fig. 21), as the chain of PEG molecule began to fold on itself, making it difficult to interact with enzymes and affecting the interactions between the substrate molecules and enzyme. Moreover, increasing the length of PEG chains might also induce the mesoscale aggregates of ILs[61,62], which interact more strongly with the protein's hydrophobic residues. As a result, both the entrance size and catalytic activity decreased when a larger molecular weight of PEG groups was used in $[PEG_{1000}(mim)_2][NTf_2]_2$. In the case of $[PEG_{200}(mim)_2][NTf_2]_2$, a largest gate distance is observed, which brings more exposure of the active site and thus a higher enzyme activity for 4-methyl-2-pentanol and 1-(1-naphthyl)ethanol. Apart from this, the maximum biocatalytic activity found in $[PEG_{200}(mim)_2][NTf_2]_2$ for these substrates might also be related with the binding affinity of ground state substrates arising from the differential enzyme–substrate interactions. Furthermore, the catalytic activity of CALB in different ILs microenvironment can't be explained alone by the conformational changes, since the existence of

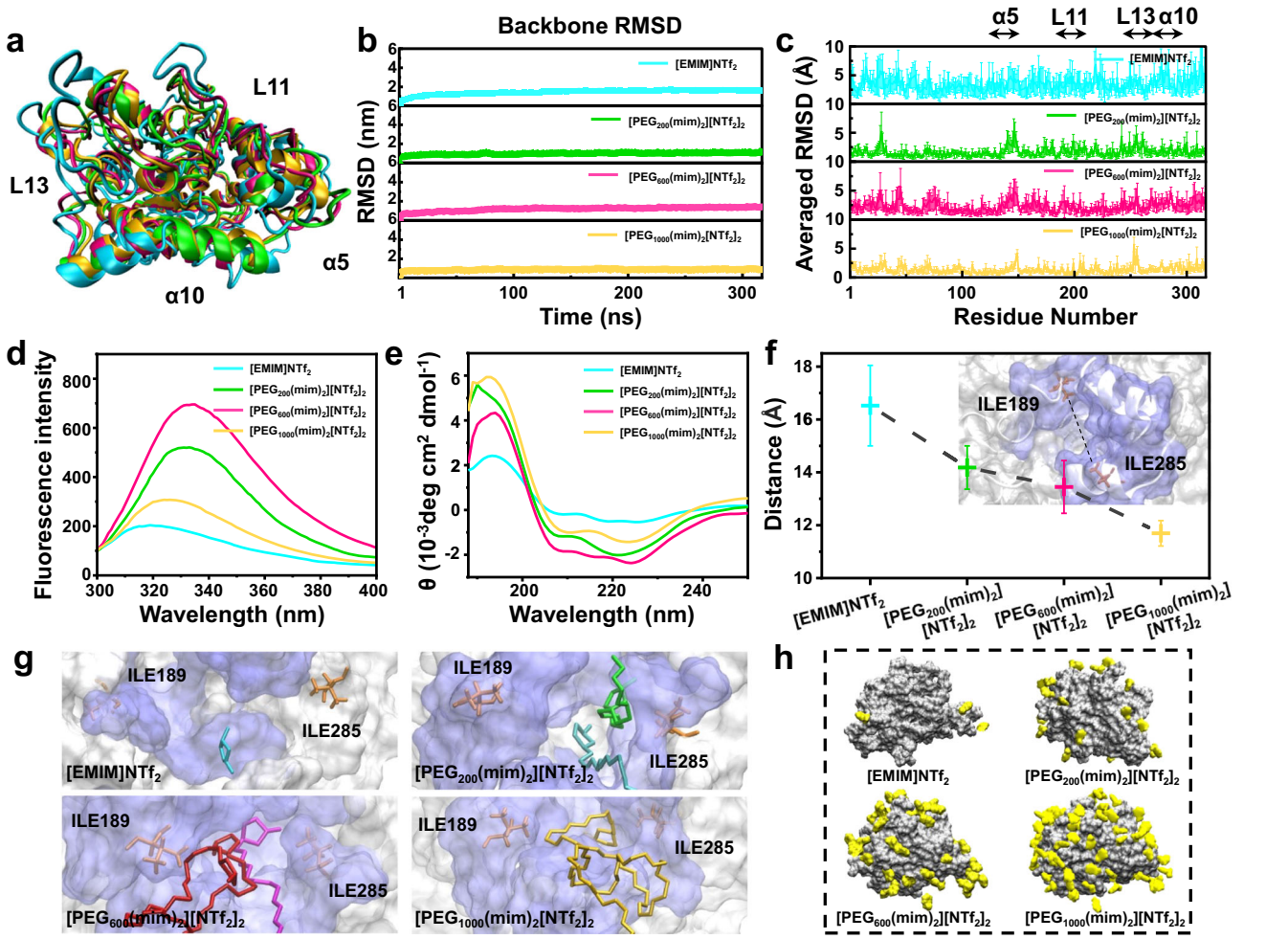

Fig. 4 | Structural analysis of CALB in different IL microenvironments. **a** Superimposed cartoon representation of the overall structures of CALB from the cluster analysis based on equilibrium trajectories drived from three independence MD simulations in each system. **b** RMSD of the enzyme backbone with respect to the initial structure as a function of time, the statistical numbers came from three independence simulations. **c** Averaged RMSD of individual residues determined from three independence simulations with the last equilibrium 100 ns trajectory for each simulation. **d** Fluorescence spectra. **e** Far-UV CD spectra. **f** Calculated width of catalytic cavity entrance between two gating residues (error bars represent standard deviation, n = three independence simulations), ILE189 and ILE285. **g** Snapshots of the active site cavity structure (derived from cluster analysis) of CALB binding with different PEG backbones. The enzyme surface is shown in gray, CALB pocket in violet, ILE189 and ILE285 in orange, and PEG backbones in green, purple or yellow. **h** Spatial distribution of substrate molecules (1-phenylethyl alcohol) occupancy at the surface of CALB from the equilibrium 100 ns in three independence simulations for each system.

unconformable situations. For example, higher catalytic activity is observed in $[PEG_{600}(mim)_2][NTf_2]_2$ while using 1-phenylethyl alcohol as substrate, though not showing the largest entrance size. Considering that the local density of substrate molecules in these ILs might also influence the catalytic activity, we then examine the simulative behavior of substrate molecules at the CALB surface. As shown in Fig. 4h and Supplementary Fig. 22, the spatial distribution images clearly show that the density of substrate molecules at the protein surface increases with increasing the PEG-molecular weight, which is consistent with the measured substrate solubility in these ILs (Supplementary Fig. 23). This increased molecular density suggests that more substrate molecules are available to the enzyme's active site and thus a possible higher enzyme activity in $[PEG_{600}(mim)_2][NTf_2]_2$.

Strengthened thermal stability

Having now established that the enzyme's structural conformation and catalytic activity could be modulated by the task-specific PEG-ILs microenvironment, we then turned to investigate the impacts of the presence of PEG groups on the thermal stability of CALB enzyme. As shown in Fig. 5a, the catalytic results of the hybrid catalyst with a PEG-IL microenvironment revealed increasing enzyme activity with evaluated temperature, reaching an optimal performance at 60 °C. While further increasing the evaluated temperature to 80 °C, the enzymatic activity reduced to some extent and the steady ee value of alcohol product decreased from 78.6% to 54.0%. Interestingly, in spite of the dropped activity, these steady values are still well maintained without significant fluctuations over a period of 320 h, suggesting the good stability at evaluated temperatures. In contrast, the PEG-free $[EMIM]NTf_2$-based catalyst showed drastically turbulent activity at 80 °C, and the CALB enzyme was almost deactivated within the same period (Fig. 5b), demonstrating the critical role of PEG groups for the thermal stabilization of the enzyme. Notably, at all evaluated temperatures, the hybrid catalyst with a PEG-IL microenvironment exhibited significantly enhanced activity compared to the PEG-free one. As presented in Fig. 5c, the SA values of PEG-IL-based catalyst was calculated to be 17.17-32.48 U mg^{-1} at different temperatures, while only 0.383-3.61 U mg^{-1} of SA values were got for the PEG-free catalyst. The persistent activity of the PEG-IL-based catalyst at extreme temperature was and likely to be complex. In this regard, we subsequently assessed the effect of PEG groups on the conformational changes of CALB by a combination of experimental methods and atomistic MD simulations. As shown in Fig. 5d, we first used temperature-dependent CD

https://doi.org/10.1038/s41467-024-54725-w

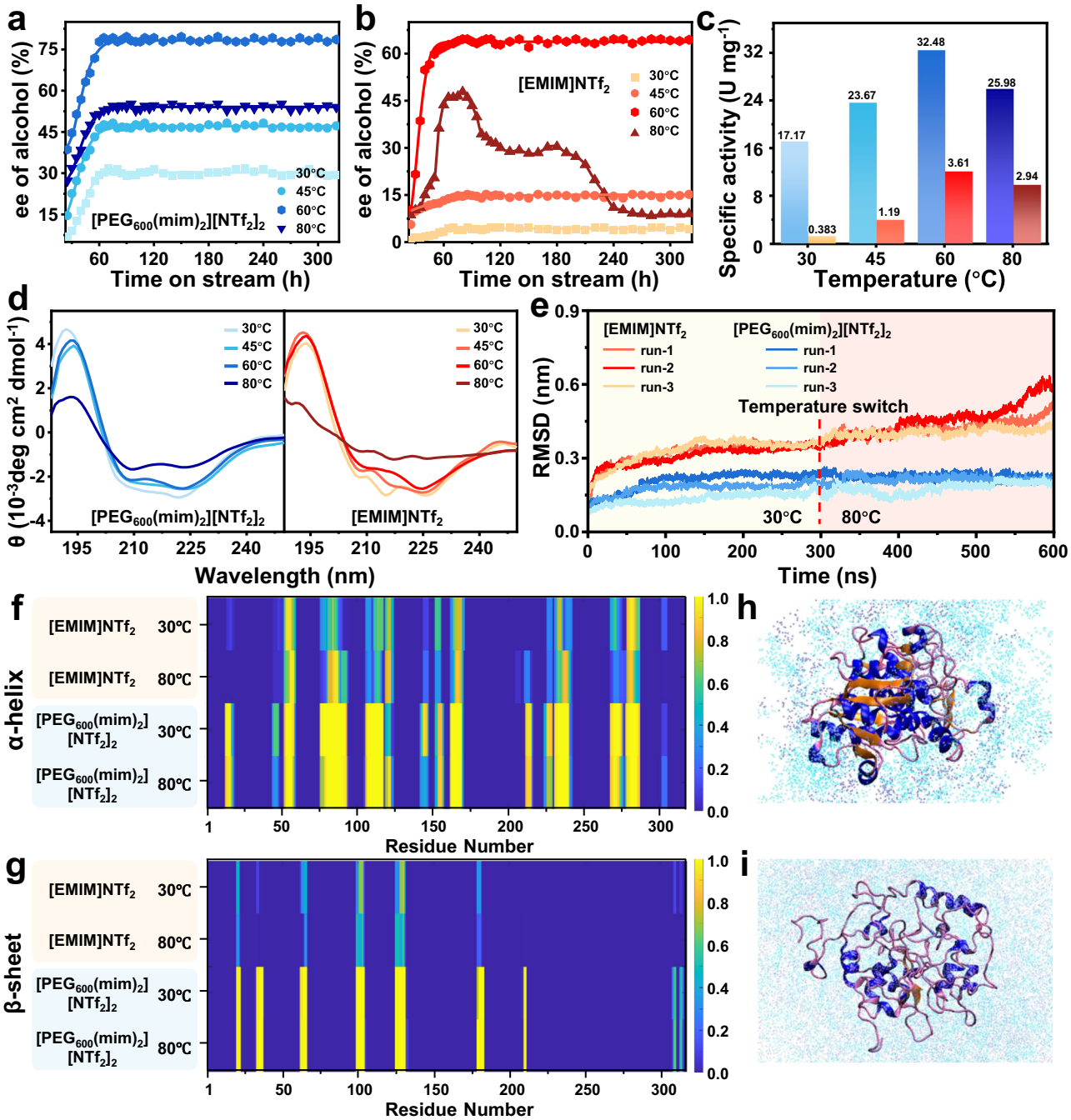

Fig. 5 | Thermal stability of CALB in different IL microenvironments. **a**, **b** Comparisons of the temperature-dependent enzymatic activity within different IL microenvironments using 1-phenylethyl alcohol as a substrate: **a** $[PEG_{600}(mim)_2][NTf_2]_2$, **b** $[EMIM]NTf_2$. **c** Specific activity of CALB in different IL microenvironments. Reaction conditions: 3.0 g hybrid catalyst, 1-phenylethyl alcohol (0.80 or 0.10 M) and vinyl acetate (3.20 or 0.40 M) in *n*-octane, flow velocity 2.0 mL h^{-1}. **d** CD spectra of CALB at different temperatures in various mediums. **e** Time evolution of RMSD for CALB in $[PEG_{600}(mim)_2][NTf_2]_2$ and $[EMIM]NTf_2$ with temperature switching from 30 °C (0-300 ns) to 80 °C (300-600 ns) in three independent simulations. **f**, **g** Secondary structures of α-helix and β-sheet for CALB in $[PEG_{600}(mim)_2][NTf_2]_2$ or $[EMIM]NTf_2$ at temperatures of 30 °C and 80 °C. **h**, **i** Snapshots in the vicinity of CALB with $[PEG_{600}(mim)_2][NTf_2]_2$ or $[EMIM]NTf_2$ as a medium at late times (at 600 ns on run−1). Only a portion of the simulation box is shown for clarity in (**h**) and (**i**), PEG groups are shown in cyan, NTf_2 ion is shown in iceblue, and substrate molecules are hidden.

spectroscopy to probe the conformational states of CALB in different microenvironments. Along with the increase of temperature from 30 to 80 °C, progressive reduction in the intensity of features at 192, 208 and 222 nm for the CALB was observed in both $[PEG_{600}(mim)_2][NTf_2]_2$ and $[EMIM]NTf_2$, indicating the existence of thermal changes in secondary structure. Significantly, the intensity reduction in $[PEG_{600}(mim)_2][NTf_2]_2$ was much lower than PEG-free $[EMIM]NTf_2$, and reflected that although the helix structures were partially denatured at 80 °C, the thermal unfolding of CALB enzyme was greatly improved in the presence of PEG groups. Then, MD simulations were also performed to clarify the effect of PEG groups on the thermal stability. For clearer presentation, we focused on the dynamics in the close vicinity of a single CALB, and the time evolution of RMSD with respect to its temperature switch from 30 °C (0-300 ns) to 80 °C (300-600 ns) in

https://doi.org/10.1038/s41467-024-54725-w

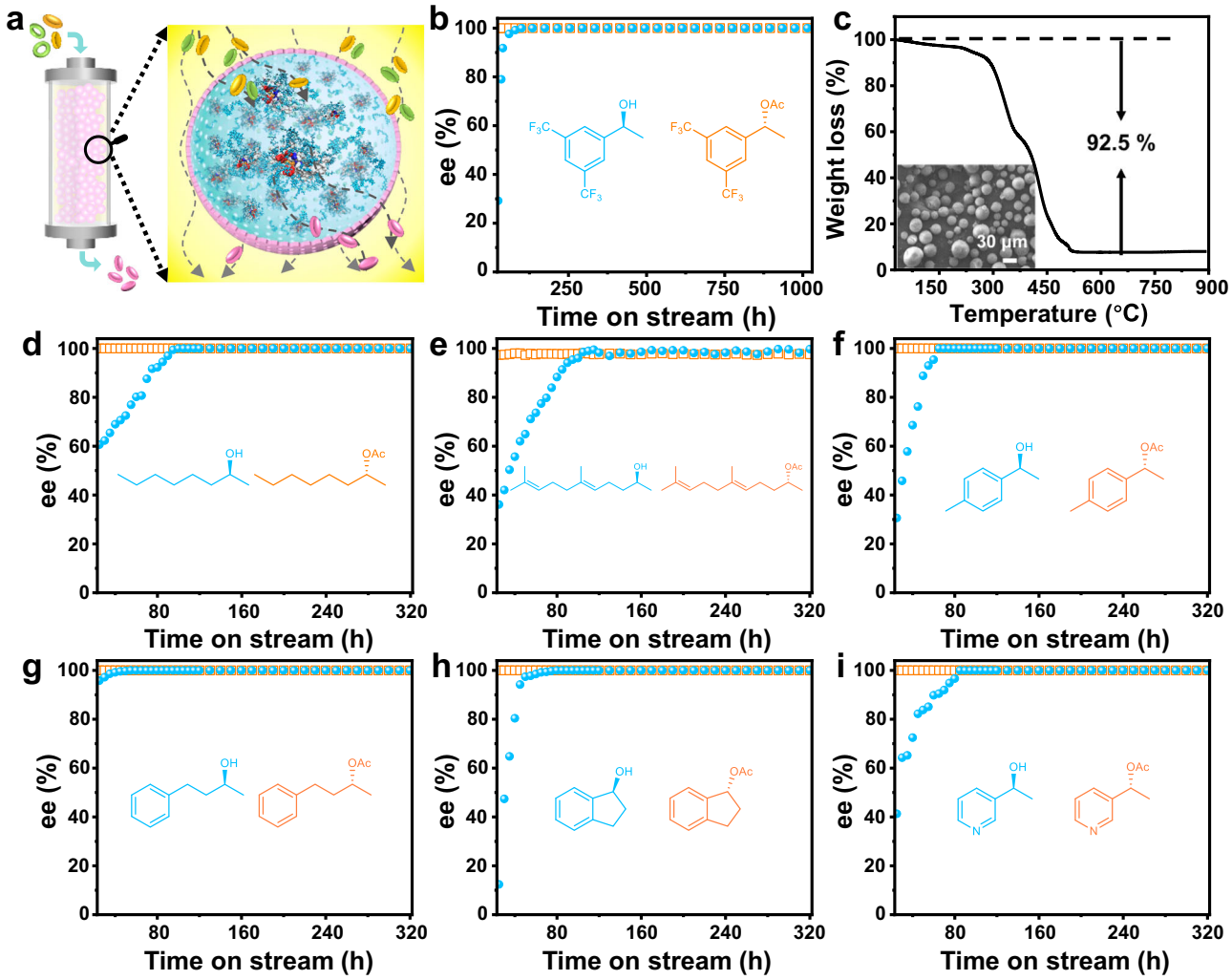

Fig. 6 | Applied performance of the PEG-IL-based microreactor in the kinetic resolution of various racemic alcohols. a Schematic illustration of the continuous-flow biocatalysis. **b** 1-(3,5-Bis(trifluoromethyl)phenyl)ethanol as a substrate. **c** TGA curve and SEM image of the hybrid catalyst after reaction. **d**–**i** Different racemic alcohols as substrates: **d** 2-octanol, **e** 6,10-dimethylundeca-5,9-dien-2-ol, **f** 1-(4-methyl phenyl)ethanol, **g** 4-phenyl-2-butanol, **h** 1-indanol, **i** 1-(pyridin-2-yl)ethanol. Reaction conditions: 3.0 g [PEG_{600}(mim)$_2$][NTf_2]$_2$-based hybrid catalyst (0.12 mg/g of enzyme loading), a solution of racemic alcohol (0.10 M) and vinyl acetate (0.40 M) in *n*-octane as the mobile phase, 60 °C, 2 mL h^{-1}.

three independent simulations (Fig. 5e) together with the corresponding secondary structure properties (Fig. 5f, g). Therein, the deviation of CALB conformation from the initial state could be quantified. For CALB in [EMIM]NTf_2, an obvious increase in RMSD and corresponding decrease in content of α-helix and β-sheet were observed at a high temperature of 80 °C compared to its counterpart at 30 °C, suggesting a large structural deviation during the temperature rising process. Notably, in the presence of PEG groups, the CALB retained its structure at evaluated temperatures, as verified by the much lower RMSD and almost unchanged content of secondary structures. Specifically, the α-helix and β-sheet remained mostly intact with only slight deviations while switching the temperature from 30 to 80 °C. Combined with the final simulation snapshots in the presence or absence of PEG groups at elevated temperatures (Fig. 5h, i and Supplementary Fig. 24), the origin for thermal stabilization of CALB enzyme in task-specific PEG-ILs can be mainly ascribed to the pronounced effect of PEG groups on stabilizing the secondary structures of CALB by delaying unfolding at high temperatures, which might be attributed to the PEG-induced H-bonding interactions that retains CALB molecules.

Applied performance for various substrates

Encouraged by the enhanced activity and excellent stability of the task-specific PEG-IL-based hybrid catalyst, we finally applied it to the kinetic resolution of a diversity of racemic alcohols in a continuous-flow manner (Fig. 6a). A pharmaceutical alcohol intermediate, 1-(3,5-bis(-trifluoromethyl)phenyl)ethanol, was first studied to verify the long-term stability. Satisfactorily, the ee values of the yielded alcohol and ester products were well maintained above 99% even after prolonging the running time to a period as long as 1000 h, highlighting a high level of practical application (Fig. 6b). The morphology and structure of the hybrid catalyst as well as its PEG-IL content were essentially unchanged after reaction, as evidenced from the SEM image and weight loss in the TGA curve of the spent catalyst (Fig. 6c and Supplementary Fig. 25). For other substrates, including racemic 2-octanol, 6,10-dimethylundeca-5,9-dien-2-ol, 1-(4-methylphenyl) ethanol, 4-phenyl-2-butanol, 1-indanol and 1-(pyridin-2-yl)ethanol, the ee values of aimed alcohols and esters were also maintained at 97-99% over a period of 320 h (Fig. 6d–i), demonstrating the good substrate scope (for mass spectrometry spectra of different alcohol and ester products, see in Supplementary Fig. 26).

Discussion

In conclusion, we have successfully constructed a task-specific PEG-IL-based liquid-solid hybrid microreactor to realize the fine engineering of structural configuration of the confined enzymes for upgrading the continuous-flow biocatalysis in practical applications. Originated from the "designer" nature of the interior PEG-IL microenvironment, not only were we able to optimize the enzymatic activity by precise altering the molecular weight of PEG groups, but also the targeted thermal stability could be strengthened so as to adapt the harsh working conditions. As exemplified by the CALB-driven kinetic resolution reaction, the power of our designed catalyst was definitely confirmed by the significantly enhanced catalytic efficiency (2.70–30.35 folds in comparison to the batch counterparts or traditional IL-based microreactors) and long-term continuous-flow stability even up to 1000 h at evaluated temperatures. Importantly, based on comprehensive understanding of the effects of PEG-IL microenvironment by combining experimental and molecular dynamics simulation studies, the underlying conformational changes of the enzyme molecule were correlated with its function alteration and the pronounced effects of PEG groups in stabilizing enzyme's secondary structures by delaying unfolding at elevated temperatures were identified. This work offers pregnant insights into the enzyme conformation activation by microenvironment engineering and provides guidelines for the rational design of robust enzyme catalysts for practical applications.

Methods

Preparation of task-specific PEG-IL-based liquid−solid hybrid microreactors

4 mL of oil phase (*n*-octane) containing silica emulsifier (80 mg) and CALB enzyme solution (53 mg; 8 mg mL^{-1} of protein; pH 8.0) was added into 2 mL task-specific PEG-IL ($[PEG_{200}(mim)_2][NTf_2]_2$, $[PEG_{600}(mim)_2][NTf_2]_2$ or $[PEG_{1000}(mim)_2][NTf_2]_2$). The biphasic mixture was vigorously sheared using a homogenizer under 10,000 rpm for 1 min, generating task-specific PEG-IL-based Pickering droplets. Then, the above enzymatic task-specific PEG-IL-based Pickering droplets were dispersed into 50 mL *n*-octane that containing 0.3 g organic linker trimethoxymethylsilane (MTMS) and 100 μL of *n*-hexylamine. The mixture was rotated on a rolling apparatus at 30 °C overnight. Then, the upper *n*-octane phase was removed and the solid products were washed with *n*-octane for several times. After drying under vacuum, the resulted enzymatic task-specific PEG-IL-based liquid−solid hybrid microreactor was redispersed in *n*-octane for the following packing in a column reactor. The preparation method of PEG-free $[EMIM]NTf_2$-based liquid−solid hybrid microreactor was similar with above.

Hybrid microreactor in continuous-flow reaction system

The enzymatic liquid-solid hybrid microreactors with $[EMIM]NTf_2$, $[PEG_{200}(mim)_2][NTf_2]_2$, $[PEG_{600}(mim)_2][NTf_2]_2$ or $[PEG_{1000}(mim)_2][NTf_2]_2$ (3.0 g) in n-octane was poured into a column reactor (inner diameter is 2 cm), whose bottom is a sand filter (4.5-9 μm in pore diameter). A solution of racemic alcohol (for example 0.1 M) and vinyl acetate (for example 0.4 M) in n-octane as mobile phase was pumped through the inlet of the column reactor at a given flow rate and was allowed to pass through the column reactor. The outflow was sampled for GC analysis at intervals.

Simulation methods

For molecular dynamics simulations, the CALB structure was derived from the Protein Data Bank, and the simulation parameters of ionic liquids and PEG were developed by Gaussian and Amber software. The isothermal-isobaric ensemble was used in our simulations, while three independent MD simulations were performed for approaching the efficient sampling. Specific molecular parameters, system modeling, MD running setup, and MD analysis details can be found in Supplementary Information.

Reporting summary

Further information on research design is available in the Nature Portfolio Reporting Summary linked to this article.

Data availability

The data for Figs. 2–6 generated in this study are provided in the Supplementary Information/Source Data file, and from corresponding author(s) upon request. Source data are provided with this paper.

References

1. Galanie, S., Thodey, K., Trenchard, I. J., Interrante, M. F. & Smolke, C. D. Complete Biosynthesis of Opioids in Yeast. *Science* **349**, 1095–1100 (2015).
2. Smith, M. R. et al. Elucidating Structure–Performance Relationships in Whole-Cell Cooperative Enzyme Catalysis. *Nat. Catal.* **2**, 809–819 (2019).
3. Wachtmeister, J. & Rother, D. Recent Advances in Whole Cell Biocatalysis Techniques Bridging from Investigative to Industrial Scale. *Curr. Opin. Biotechnol.* **42**, 169–177 (2016).
4. Bell, E. L. et al. Biocatalysis. *Nat. Rev.* **1**, 46 (2021).
5. Küchler, A., Yoshimoto, M., Luginbühl, S., Mavelli, F. & Walde, P. Enzymatic Reactions in Confined Environments. *Nat. Nanotechnol.* **11**, 409–420 (2016).
6. Guindani, C., Da Silva, L. C., Cao, S., Ivanov, T. & Landfester, K. Synthetic Cells: from Simple Bio-inspired Modules to Sophisticated Integrated Systems. *Angew. Chem. Int. Ed.* **61**, e202110855 (2022).
7. Marguet, M., Bonduelle, C. & Lecommandoux, S. Multicompartmentalized Polymeric Systems: Towards Biomimetic Cellular Structure and Function. *Chem. Soc. Rev.* **42**, 512–529 (2013).
8. Cook, A. B., Novosedlik, S. & Van Hest, J. C. M. Complex Coacervate Materials as Artificial Cells. *Acc. Mater. Res.* **4**, 287–298 (2023).
9. Jeong, S., Nguyen, H. T., Kim, C. H., Ly, M. N. & Shin, K. Toward Artificial Cells: Novel Advances in Energy Conversion and Cellular Motility. *Adv. Funct. Mater.* **30**, 1907182 (2020).
10. Shang, L. R., Ye, F. F., Li, M. & Zhao, Y. J. Spatial Confinement toward Creating Artificial Living Systems. *Chem. Soc. Rev.* **51**, 4075–4093 (2022).
11. Bornscheuer, U. T. Immobilizing Enzymes: How to Create More Suitable Biocatalysts. *Angew. Chem. Int. Ed.* **42**, 3336–3337 (2003).
12. Wang, Y., Zhao, Q., Haag, R., Wu, C. Z. Biocatalytic Synthesis Using Self-Assembled Polymeric Nano- and Microreactors. *Angew. Chem. Int. Ed.* e202213974 (2022).
13. Tamasi, M. J. et al. Machine Learning on a Robotic Platform for the Design of Polymer–Protein Hybrids. *Adv. Mater.* **34**, 2201809 (2022).
14. Zhang, Y. F., Ge, J. & Liu, Z. Enhanced Activity of Immobilized or Chemically Modified Enzymes. *ACS Catal.* **5**, 4503–4513 (2015).
15. González, M. V., Wang, C. & Willner, I. Biocatalytic Cascades Operating on Macromolecular Scaffolds and in Confined Environments. *Nat. Catal.* **3**, 256–273 (2020).
16. Klibanov, A. M. Improving Enzymes by Using Them in Organic Solvents. *Nature* **409**, 241–246 (2001).
17. Stepankova, V. et al. Strategies for Stabilization of Enzymes in Organic Solvents. *ACS Catal.* **3**, 2823–2836 (2013).
18. Corma, A., Fornes, V. & Rey, F. Delaminated Zeolites: An Efficient Support for Enzymes. *Adv. Mater.* **14**, 71–74 (2002).
19. Liu, J., Yang, Q. H. & Li, C. Towards Efficient Chemical Synthesis via Engineering Enzyme Catalysis in Biomimetic Nanoreactors. *Chem. Commun.* **51**, 13731–13739 (2015).
20. Filice, M. & Palomo, J. M. Cascade Reactions Catalyzed by Bionanostructures. *ACS Catal.* **4**, 1588–1598 (2014).
21. Engström, K. et al. Co-immobilization of an Enzyme and a Metal into the Compartments of Mesoporous Silica for Cooperative Tandem Catalysis: An Artificial Metalloenzyme. *Angew. Chem. Int. Ed.* **52**, 14006–14010 (2013).

22. Liang, W. et al. Metal–Organic Framework-Based Enzyme Biocomposites. *Chem. Rev.* **121**, 1077–1129 (2021).
23. Wang, X., Lan, P. C. & Ma, S. Metal–Organic Frameworks for Enzyme Immobilization: Beyond Host Matrix Materials. *ACS Cent. Sci.* **6**, 1497–1506 (2020).
24. Huang, S. M., Kou, X. X., Shen, J., Chen, G. S. & Ouyang, G. F. Armor-Plating" Enzymes with Metal-Organic Frameworks (MOFs). *Angew. Chem. Int. Ed.* **59**, 8786–8798 (2020).
25. Zhang, J. et al. The Encounter of Biomolecules in Metal–Organic Framework Micro/Nano Reactors. *ACS Appl. Mater. Interfaces* **13**, 52215–52233 (2021).
26. Qiao, S., Jin, H. Q., Zuo, A. L. & Chen, Y. Integration of Enzyme and Covalent Organic Frameworks: From Rational Design to Applications. *Acc. Chem. Res.* **57**, 93–105 (2024).
27. Xing, C. Y. et al. Enhancing Enzyme Activity by the Modulation of Covalent Interactions in the Confined Channels of Covalent Organic Frameworks. *Angew. Chem. Int. Ed.* **61**, e202201378 (2022).
28. Sun, Q. et al. Pore Environment Control and Enhanced Performance of Enzymes Infiltrated in Covalent Organic Frameworks. *J. Am. Chem. Soc.* **140**, 984–992 (2018).
29. Lancaster, L., Abdallah, W., Banta, S. & Wheeldon, I. Engineering Enzyme Microenvironments for Enhanced Biocatalysis. *Chem. Soc. Rev.* **47**, 5177–5186 (2018).
30. Li, Y. M. et al. Fine-Tuning the Micro-Environment to Optimize the Catalytic Activity of Enzymes Immobilized in Multivariate Metal –Organic Frameworks. *J. Am. Chem. Soc.* **143**, 15378–15390 (2021).
31. Chen, G. S. et al. Hydrogen-bonded Organic Framework Biomimetic Entrapment Allowing Non-native Biocatalytic Activity in Enzyme. *Nat. Commun.* **13**, 4816 (2022).
32. Hartley, C. J. et al. Engineered Enzymes that Retain and Regenerate Their Cofactors Enable Continuous-Flow Biocatalysis. *Nat. Catal.* **2**, 1006–1015 (2019).
33. Itoh, T. Ionic Liquids as Tool to Improve Enzymatic Organic Synthesis. *Chem. Rev.* **117**, 10567–10607 (2017).
34. Sheldon, R. A. Biocatalysis in Ionic Liquids: State-of-the-Union. *Green. Chem.* **23**, 8406–8427 (2021).
35. Lau, R. M. et al. Dissolution of Candida Antarctica Lipase B in Ionic Liquids: Effects on Structure and Activity. *Green. Chem.* **6**, 483–487 (2004).
36. Sanchez-Fernandez, A. et al. Hydration in Deep Eutectic Solvents Induces Non-Monotonic Changes in the Conformation and Stability of Proteins. *J. Am. Chem. Soc.* **144**, 23657–23667 (2022).
37. Lozano, P., De Diego, T., Larnicol, M., Vaultier, M. & Iborra, J. L. Chemoenzymatic Dynamic Kinetic Resolution of Rac-1-phenylethanol in Ionic Liquids and Ionic Liquids/Supercritical Carbon Dioxide Systems. *Biotechnol. Lett.* **28**, 1559–1565 (2006).
38. Brogan, A. P. S., Bui-Le, L. & Hallett, J. P. Non-aqueous Homogenous Biocatalytic Conversion of Polysaccharides in Ionic Liquids using Chemically Modified Glucosidase. *Nat. Catal.* **10**, 859–865 (2018).
39. Abe, Y., Yagi, Y., Hayase, S., Kawatsura, M. & Itoh, T. Ionic Liquid Engineering for Lipase-Mediated Optical Resolution of Secondary Alcohols: Design of Ionic Liquids Applicable to Ionic Liquid Coated-Lipase Catalyzed Reaction. *Ind. Eng. Chem. Res.* **51**, 9952–9958 (2012).
40. Villa, R. et al. Ionic Liquids as an Enabling Tool to Integrate Reaction and Separation Processes. *Green. Chem.* **21**, 6527–6544 (2019).
41. Lozano, P., De Diego, T., Carrie, D., Vaultier, M. & Iborra, J. L. Overstabilization of Candida antarctica Lipase B by Ionic Liquids in Ester Synthesis. *Biotech. Lett.* **23**, 1529–1533 (2001).
42. Zhang, M. et al. Ionic Liquid Droplet Microreactor for Catalysis Reactions Not at Equilibrium. *J. Am. Chem. Soc.* **139**, 17387–17396 (2017).
43. Imam, H. T. et al. Supramolecular Ionic Liquid Gels for Enzyme Entrapment. *ACS Sustain. Chem. Eng.* **11**, 6829–6837 (2023).
44. Pérez-Tomás, J. Á. et al. Entrapment in HydrIL gels: Hydro-Ionic Liquid Polymer Gels for Enzyme Immobilization. *Catal. Today* **432**, 114595 (2024).
45. Zhang, X. M. et al. Pickering Emulsion-Derived Liquid–Solid Hybrid Catalyst for Bridging Homogeneous and Heterogeneous Catalysis. *J. Am. Chem. Soc.* **141**, 5220–5230 (2019).
46. Itoh, T. et al. Increased Enantioselectivity and Remarkable Acceleration of Lipase-Catalyzed Transesterification by Using an Imidazolium PEG–Alkyl Sulfate Ionic Liquid. *Chem. Eur. J.* **12**, 9228–9237 (2006).
47. Zhao, H., Jones, C. L. & Cowins, J. V. Lipase Dissolution and Stabilization in Ether-Functionalized Ionic Liquids. *Green. Chem.* **11**, 1128–1138 (2009).
48. Li, X., Zhang, C., Li, S., Huang, H. & Hu, Y. Improving Catalytic Performance of Candida rugosa Lipase by Chemical Modification with Polyethylene Glycol Functional Ionic Liquids. *Ind. Eng. Chem. Res.* **54**, 8072–8079 (2015).
49. Ameloot, R. et al. Interfacial Synthesis of Hollow Metal-Organic Framework Capsules Demonstrating Selective Permeability. *Nat. Chem.* **3**, 382–387 (2011).
50. Fach, M., Radi, L. & Wich, P. R. Nanoparticle Assembly of Surface-Modified Proteins. *J. Am. Chem. Soc.* **138**, 14820–14823 (2016).
51. Wang, X. et al. Polyethylene Glycol Crowder's Effect on Enzyme Aggregation, Thermal Stability, and Residual Catalytic Activity. *Langmuir* **37**, 8474–8485 (2021).
52. Verho, O. & Bäckvall, J. E. Chemoenzymatic Dynamic Kinetic Resolution: A Powerful Tool for the Preparation of Enantiomerically Pure Alcohols and Amines. *J. Am. Chem. Soc.* **137**, 3996–4009 (2015).
53. Yang, T., Zhang, Y. F., Wang, J., Huang, F. H. & Zheng, M. M. Magnetic Switchable Pickering Interfacial Biocatalysis: One-Pot Cascade Synthesis of Phytosterol Esters from High-Acid Value Oil. *ACS Sustain. Chem. Eng.* **9**, 12070–12078 (2021).
54. Yang, T. et al. pH-Switchable Pickering Interfacial Biocatalysis: One-Pot Enzymatic Synthesis of Phytosterol Esters with Low-Value Rice Bran Oil. *ACS Sustain. Chem. Eng.* **10**, 6963–6972 (2022).
55. Dong, Z. et al. Carbon Nanoparticle-Stabilized Pickering Emulsion as a Sustainable and High-Performance Interfacial Catalysis Platform for Enzymatic Esterification/Transesterification. *ACS Sustain. Chem. Eng.* **7**, 7619–7629 (2019).
56. Zhong, H. Y. et al. Ultraviolet/Visible Light-Responsive Pickering Interfacial Biocatalysis: Efficient and Robust Platform for Bioconversions. *ACS Sustain. Chem. Eng.* **12**, 1857–1867 (2024).
57. Kim, H. S., Ha, S. H., Sethaphong, L., Koo, Y. M. & Yingling, Y. G. The Relationship between Enhanced Enzyme Activity and Structural Dynamics in Ionic Liquids: A Combined Computational and Experimental Study. *Phys. Chem. Chem. Phys.* **16**, 2944–2953 (2014).
58. Banik, S. D., Nordblad, M., Woodley, J. M. & Peters, G. H. A Correlation between the Activity of Candida antarctica Lipase B and Differences in Binding Free Energies of Organic Solvent and Substrate. *ACS Catal.* **6**, 6350–6361 (2016).
59. Kim, H. S., Eom, D., Koo, Y. M. & Yingling, Y. G. The Effect of Imidazolium Cations on the Structure and Activity of the Candida Antarctica Lipase B Enzyme in Ionic Liquids. *Phys. Chem. Chem. Phys.* **18**, 22062–22069 (2016).
60. Diego, T. D., Lozano, P., Gmouh, S., Vaultier, M. & Iborra, J. L. Understanding Structure-Stability Relationships of Candida Antartica Lipase B in Ionic Liquids. *Biomacromolecules* **6**, 1457–1464 (2005).
61. Dong, K., Liu, X. M., Dong, H. F., Zhang, X. P. & Zhang, S. J. Multiscale Studies on Ionic Liquids. *Chem. Rev.* **117**, 6636–6695 (2017).
62. Gomes, M. F. C., Lopes, J. N. C. & Padua, A. A. H. Thermodynamics and Micro Heterogeneity of Ionic Liquids. *Top. Curr. Chem.* **290**, 161–183 (2009).

Acknowledgements
This work is supported by the National Key Research and Development Program of China (2021YFC2101900), the Natural Science Foundation of China (22072078, 21925203), the Outstanding Youth Fund of Shanxi Province (202103021222003).

Author contributions
H.Q.Y. and X.M.Z. conceived and supervised the project; X.T.H. and Z.Q.M. executed the experiments and collected the data; H.S. and S.W. conducted the theoretical calculations; M.Z. contributed in discussing and analyzing the results. X.M.Z. wrote the paper. All authors edited the paper.

Competing interests
The authors declare no competing interests.

Additional information
Supplementary information The online version contains supplementary material available at https://doi.org/10.1038/s41467-024-54725-w.

Correspondence and requests for materials should be addressed to Xiaoming Zhang, Hu Shi or Hengquan Yang.

Peer review information *Nature Communications* thanks To Ngai, Emel Timucin, Mingming Zheng and the other, anonymous, reviewer(s) for their contribution to the peer review of this work. A peer review file is available.